Applied Surface Science 300 (2014) 58–65

Contents lists available at ScienceDirect

Applied Surface Science

journal homepage: www.elsevier.com/locate/apsusc

Catalytic oxidation of NO with O_2 over $FeMnO_x/TiO_2$: Effect of iron and manganese oxides loading sequences and the catalytic mechanism study

Mengying Zhang[a,b], Caiting Li[a,b,*], Long Qu[a,b], Mengfan Fu[a,b], Guangming Zeng[a,b], Chunzhen Fan[a,b], Jinfeng Ma[a,b], Fuman Zhan[a,b]

[a] College of Environmental Science and Engineering, Hunan University, Changsha 410082, China
[b] Key Laboratory of Environmental Biology and Pollution Control (Hunan University), Ministry of Education, Changsha 410082, China

ARTICLE INFO

Article history:
Received 13 January 2014
Accepted 3 February 2014
Available online 16 February 2014

Keywords:
NO oxidation
$FeMnO_x/TiO_2$
Loading sequences
Mechanism

ABSTRACT

$FeMnO_x/TiO_2$ with different iron and manganese oxides adding orders were prepared through isovolumetric impregnation and tested for catalytic oxidation of NO with O_2. It was found that the sample obtained from one-step impregnation method had better catalytic activity. The excellent activity was attributed to higher surface area, lower crystalline of manganese oxides, abundant Mn^{3+}, Fe^{3+} and chemisorbed oxygen species on the surface. Furthermore, effects of loading sequences on $FeMnO_x/TiO_2$ catalysts were investigated. The study showed that Fe and Mn would affect each other and change the surface physicochemical properties of $FeMnO_x/TiO_2$ when they were loaded step-by-step. In addition, the inhibiting effect of H_2O on catalytic activity was reversible while the conversion of NO recovered to 40% when SO_2 was cut off. XPS analysis between used and fresh catalysts revealed the electron transfer between Fe^{n+} and Mn^{n+} ions in $FeMnO_x/TiO_2$. Possible reaction mechanism was put forward by comprehensive analysis of XPS and FT-IR results.

1. Introduction

Nitrogen oxides (NO_x) which mainly contain nitric oxide (NO) and nitrogen dioxide (NO_2), contribute to many environmental problems such as acid rain ozone depletion and photochemical smog [1–3]. NO_x removal has been urgently required due to the increasing emission from transport sectors and industries. Considerable interest has recently been taken into the process of developing catalysts for oxidizing NO into NO_2, since NO_2 is always more favored than NO for NO_x reduction among several procedures such as selective catalytic reduction with hydrocarbons (HC-SCR) [4] or ammonia (NH_3-SCR) [4–6] and NO_x storage-reduction (NSR) [4,7,8]. Besides that NO_2 is easier to be removed by absorption than NO. The maximum NO_x absorption efficiency could be achieved while the ratio of NO/NO_x equals about 60% [3,9–11]. As the percentage of NO in NO_x is more than 90%, one promising approach to oxidize NO to more actively NO_2 ($2NO + O_2 \rightarrow 2NO_2$) in either gas or liquid phase is needed [3,10].

Manganese oxide (MnO_x) has attracted lots concerns for NO_x reduction since the year of 1994 when MnO_x was firstly used in SCR by Kapteijn et al. [12]. Nowadays, MnO_x is widely used in NO oxidation due to their high catalytic efficiency and fairly cost-effective. Effects of Mn precursors [13] and preparation methods [14] on NO oxidation over Mn/TiO_2 have been studied. Tang et al. [15] deduced the mechanism of NO catalytic oxidation over MnO_x/TiO_2 catalyst through a systematic in situ diffuse reflectance infrared Fourier transform spectroscopy (DRIFTS) investigation. A few works found that catalytic oxidation of NO to NO_2 would happen when Mn–Fe composite oxides was used in selective catalytic reduction of NO by NH_3 [16–19]. Chen et al. [18] indicated that adding Fe on MnO_x could increase the activity for NO oxidation to NO_2 and thereby enhance the SCR activity. Yang et al. [19] reported that Fe^{3+} cation on the surface over Mn–Fe spinel would oxidize the adsorbed NO to form NO_2^- during the SCR reaction. Zhao et al. [17] also found the addition of Fe increased both NO conversion and the resistance to H_2O and SO_2 for $Fe–La–Mn/Al_2O_3$. $FeMnO_x$-based catalysts were expected to perform well for NO oxidation which they were rarely used for [20].

* Corresponding author at: College of Environmental Science and Engineering, Hunan University, Changsha 410082, China. Tel.: +86 731 88649216; fax: +86 731 88649216.
E-mail addresses: ctli@hnu.edu.cn, ctli3@yahoo.com (C. Li).

http://dx.doi.org/10.1016/j.apsusc.2014.02.002
0169-4332/

Impregnation method is widely used in preparation for supported metal oxide catalysts. When two or more active components are loaded on the supported materials, the precursors are usually added simultaneously. Few works have been done to check out whether the active components affect each other when they are added step-by-step [21]. This work focused on the comparison of $FeMnO_x/TiO_2$ catalysts which were synthesized with different adding orders by isovolumetric impregnation method. Effects of loading sequences on the physicochemical properties of catalysts were systematically investigated by N_2 adsorption–desorption, powder X-ray diffraction (XRD), scanning electron microscopy (SEM), X-ray photoelectron spectra (XPS) in combination with the activity evaluation of NO catalytic conversion. Sulfur and water resistance tests on the best performed catalyst have also been carried out. Mechanism of such a heterogeneous reaction was deduced through XPS and Fourier-transform infrared spectra (FT-IR) analysis in present work.

2. Experiment

2.1. Materials preparation

The molar ratios of Fe/Ti and Mn/Ti were 0.15 and 0.3, respectively, as Fe(0.15)–Mn(0.3)/TiO_2 had the best performance in oxidation of NO (Figs. S1 and S2). The commercial titanium dioxide (TiO_2) was obtained from Tianjin Kemiou Chemical Reagent Co. Ltd. (Tianjin, China). All the chemicals were of analytical grade and used as received without further purification.

Mn(0.3)/TiO_2 and Fe(0.15)/TiO_2 were prepared by isovolumetric impregnation method. Before the addition of TiO_2, appropriate amount of manganese nitrate or ferric nitrate was added to deionized water in a beaker with steady stirring at 30 °C. The duration time meeting the requirement of immersion was 24 h. The mixtures obtained after impregnation were dried overnight at 110 °C and calcined at 450 °C for 3 h before they were ground into particles.

Mn(0.3)/Fe(0.15)/TiO_2 and Fe(0.15)/Mn(0.3)/TiO_2 were synthesized by adding Fe(0.15)/TiO_2 and Mn(0.3)/TiO_2 particles into the solution of manganese nitrate and ferric nitrate, respectively. The Mn(0.3)–Fe(0.15)/TiO_2 catalyst was prepared by adding TiO_2 into the mixed manganese nitrate and ferric nitrate solution. The procedures were the same as above. TiO_2 sample impregnated with deionized water was prepared by the same way.

2.2. Characterization of materials

The specific surface areas of samples were determined by nitrogen adsorption–desorption at −196 °C on a Quadrasorb SI-3MP analyzer (Quantachrome Instruments, USA). The specific surface area was determined by BET (Brunauer–Emmett–Teller) equation in 0.05–0.35 partial pressure range. Pore volumes and average pore diameters were determined by Barrett–Joyner–Halenda (BJH) method from the desorption branches of the isotherms.

XRD measurements were carried out on Rotaflex D/Max-C powder diffractometer (Rigaku, Japan) to examine the crystallinity and dispersivity of manganese and iron species on TiO_2. The XRD patterns were obtained over the 2θ range from 10 to 80° with 2° min^{-1} scanning rate and 0.02° data interval, using nickel-filtered Cu Kα (λ = 0.1543 nm) radiation as an X-ray source.

XPS analysis was performed at room temperature on a K-Alpha 1063 X-ray photoelectron spectrometer (Thermo Fisher Scientific, USA) using 72 W Al Kα radiation from micro-aggregation monochromator. The penetration depth of the XPS was 10 nm. The binding energies were calibrated by the C 1s peak at 284.6 eV.

SEM photographs were obtained by means of Hitachi S-4800 (Hitachi Limited, Japan). The separated areas for each sample were magnified to 40 000× and 100 000×.

FT-IR spectra were recorded on a FTIR-8400S IR Prestige-21 (Shimadzu, Japan) apparatus with a resolution factor of 2 cm^{-1} from 400 to 4000 cm^{-1}, while the scans were collected at a scan speed of 5 kHz. The pre-treated sample was first mixed with KBr at a ratio of 1/100 (by weight) at each test. Background spectrum of pure KBr was recorded and subtracted from each sample spectrum.

2.3. Catalytic activity testing

Catalytic activity tests of NO oxidation with O_2 were carried out in a vertically oriented stainless steel column at 80–480 °C under atmospheric pressure. The catalysts (1.0 g) were packed between two pieces of glass wood which were plugged up to ensure the material layer was in the center of the reactor. Standard composition of the basic flue gas included 500 ppm NO, 5% O_2, 4 vol% H_2O (when used), 200 ppm SO_2 (when used) and balanced N_2. The total flow rate was kept at 0.3 L/min, corresponding to a gas hourly space velocity (GHSV) of 15 000 h^{-1}. The peristaltic pump transferred water into the stainless steel tube wrapped with a heating line and then H_2O (g) was generated. Before entering the reactor, feed gases were mixed in a mixing tank, while O_2 was fed directly into the reactor to avoid possible reaction with NO and SO_2 upstream the catalyst layer.

Concentrations of NO, NO_2 and SO_2 were measured by a flue gas analyzer (Testo 350 XL, Testo Co., Germany). The NO oxidation conversion was calculated by the following equation:

$$\text{NO oxidation conversion}\,(\%) = \frac{100\% \times (C^0_{NO} - C_{NO})}{C^0_{NO}}$$

where C_{NO} is the outlet NO concentration (ppm) and C^0_{NO} is the inlet NO concentration (ppm).

3. Results and discussion

3.1. Effect of iron and manganese oxides loading sequences on physicochemical property of the catalysts

3.1.1. Catalytic performance for NO oxidation

The temperature dependence of steady-state NO oxidation over various materials were measured and compared with the thermodynamic equilibrium for NO conversion to NO_2 (in dashed) under the given conditions (Fig. 1). TiO_2 showed negligible catalytic activity during the entire temperature, while reactions on the other catalysts were kinetically limited at low temperature and became thermodynamic controlled after the equilibrium curve was reached.

After the addition of Mn to TiO_2 and Fe(0.15)/TiO_2, the catalytic activity exhibited great enhancement, and the peaks removed to lower temperature. However, the change was not so obvious when Fe was loaded on TiO_2 and Mn(0.3)/TiO_2. Mn brought a bigger improvement for catalytic activity on NO oxidation than Fe did, especially for the promotion of NO oxidation at low temperature. Fe(0.15)–Mn(0.3)/TiO_2 exhibited the highest catalytic activity, with the maximum NO conversion of 70% at 320 °C. In contrast, the removal efficiency of NO at the same temperature was lower when the catalyst was obtained by step-by-step impregnation. These results indicated that loading sequences influenced the activity of $MnFeO_x/TiO_2$, and one-step impregnation was favorable for improving the catalytic activity.

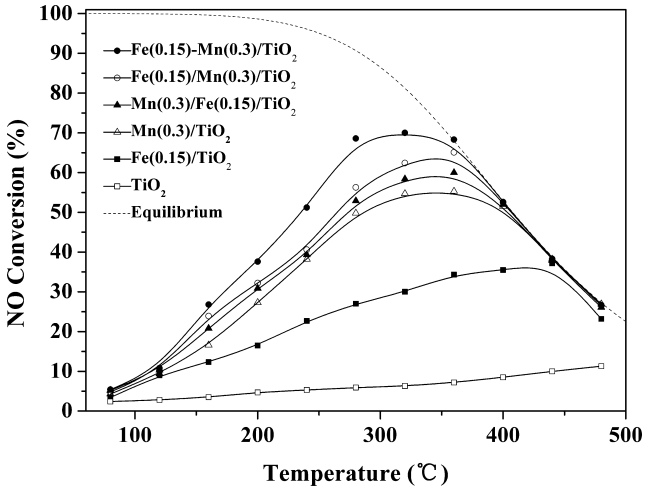

Fig. 1. NO conversion over $FeMnO_x/TiO_2$ catalysts of different iron and manganese oxides loading sequences. Reaction conditions: 1.0 g sample, 500 ppm NO, 5% O_2, N_2 balanced; GHSV = 15 000 h^{-1}.

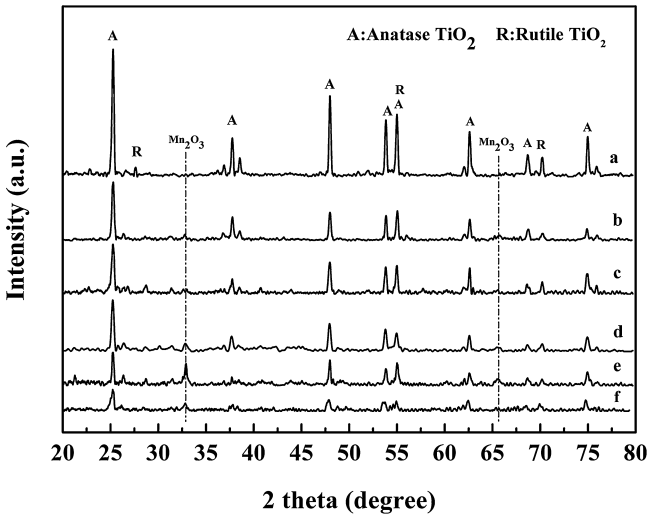

Fig. 2. XRD patterns of the catalysts: (a) TiO_2, (b) $Mn(0.3)/TiO_2$, (c) $Fe(0.15)/TiO_2$, (d) $Fe(0.15)–Mn(0.3)/TiO_2$, (e) $Mn(0.3)/Fe(0.15)/TiO_2$, (f) $Fe(0.15)/Mn(0.3)/TiO_2$.

3.1.2. BET analysis

The BET specific surface area, pore volumes and average pore sizes of different catalysts were summarized in Table 1. The specific surface areas increased in the following sequence: $Mn(0.3)/Fe(0.15)/TiO_2 < Mn(0.3)/TiO_2 < TiO_2 < Fe(0.15)/TiO_2 < Fe(0.15)/Mn(0.3)/TiO_2 < Fe(0.15)–Mn(0.3)/TiO_2$, which was not in corresponding with the trend of the NO oxidation activity. Although it was reported that bigger surface area could provide more active sites for catalytic reaction [13], surface area was not the determinant factor of the catalytic activities for oxidation of NO.

The influence of loading sequence to the tertiary oxides catalyst was also investigated. Among all the samples, $Fe(0.15)–Mn(0.3)/TiO_2$ possessed the largest specific surface area (17.93 m^2/g). The addition of Mn reduced the surface areas of catalysts. This phenomenon could also be found in $Mn(0.3)/TiO_2$ and $Mn(0.3)/Fe(0.15)/TiO_2$ whose surface areas were 11.06 m^2/g and 9.432 m^2/g, respectively. Combined with the XRD results discussed later, it could be inferred that MnO_x occupied a part of free pores of carriers during the impregnation process, and step-by-step impregnation with prior addition of Fe to TiO_2 would intensify the effect. For the samples $Fe(0.15)/TiO_2$ and $Fe(0.15)/Mn(0.3)/TiO_2$, the surface areas and pore volumes of the carriers were both greatly increased after the addition of Fe. The results suggested that Fe could improve the pore volumes of the carriers and increase the specific surface areas as well.

3.1.3. XRD analysis

XRD was used to investigate the phase structures of the samples (Fig. 2). Crystalline phases associated with TiO_2 support could be clearly observed for all the samples. There were many peaks (25.3°, 37.8°, 48.0°, 53.9°, and 55.1°) corresponded to anatase TiO_2 (ICDD #21-1272) and only a few peaks (27.4° and 54.3°) were rutile TiO_2 (ICDD #21-1276). With Fe and Mn loading, TiO_2 peaks were still clearly observed but their intensity decreased, which suggested that Mn and Fe had interacted with TiO_2 and covered the surface of TiO_2 [22].

$Mn(0.3)/TiO_2$ showed small peaks at 32.95° and 65.8° (ICDD #41-1442) which belonged to crystalline Mn_2O_3. The diffraction peak of Mn_2O_3 phase became sharp in $Mn(0.3)/Fe(0.15)/TiO_2$, but changed a little for $Fe(0.15)/Mn(0.3)/TiO_2$ and $Fe(0.15)–Mn(0.3)/TiO_2$. It could be preliminarily inferred that the existence of Fe on the surface of catalyst increased the crystallinity of Mn oxides [16]. Therefore, the highest activity of $Fe(0.15)–Mn(0.3)/TiO_2$ was partly due to the well distribution of manganese on the support [13].

For all the samples, no obvious traces of FeO_x were found in any of the catalysts during XRD analysis, which clearly indicated that FeO_x species were well dispersed throughout the support structure or their crystalline structures were too small to detect [13,23,24].

Table 1
BET surface areas and pore parameters of different catalysts.

Samples	Surface area (m^2/g)	Pore volume (cm^2/g)	Average pore size (nm)
TiO_2	13.46	0.047	3.433
$Mn(0.3)/TiO_2$	11.06	0.054	3.937
$Fe(0.15)/TiO_2$	16.4	0.063	20.88
$Fe(0.15)–Mn(0.3)/TiO_2$	17.93	0.066	29.532
$Mn(0.3)/Fe(0.15)/TiO_2$	9.432	0.018	3.079
$Fe(0.15)/Mn(0.3)/TiO_2$	16.581	0.071	13.615

3.1.4. SEM analysis

To further analyze the morphology and surface structure of the samples, SEM images of $FeMnO_x/TiO_2$ catalysts were obtained and compared with virgin TiO_2 (Fig. 3). The separated areas for each sample were magnified to 40 000 multiplier (Fig. 3A) and 100 000 multiplier (Fig. 3B).

As shown in Fig. 3, the characteristics of the TiO_2 surface have changed according to the chemical loading. For $Fe(0.15)–Mn(0.3)/TiO_2$, the metal oxides on the TiO_2 surface was highly dispersed and only a few oxides agglomerates existed in TiO_2. While the metal oxides particles were much bigger on the surface of the other catalysts, which indicated that the agglomerate were more apparent for $Fe(0.15)/Mn(0.3)/TiO_2$ and $Mn(0.3)/Fe(0.15)/TiO_2$. The results were in accordance with the XRD results. It could be seen that $Fe(0.15)/Mn(0.3)/TiO_2$ catalyst possessed a better smooth and uniform particle size distribution than $Mn(0.3)/Fe(0.15)/TiO_2$. Therefore, adding Fe before Mn would prevent the dispersion of MnO_x. The addition of Fe could enhance the active species dispersed over catalyst support, which would improve the surface area of catalyst.

3.1.5. XPS analysis

In order to found out the influence of loading sequences on the surface chemical states of catalysts, XPS spectra of Mn 2p, Fe 2p and O 1s in ternary composite catalysts were obtained. Surface atom concentrations obtained by XPS characterization were shown in

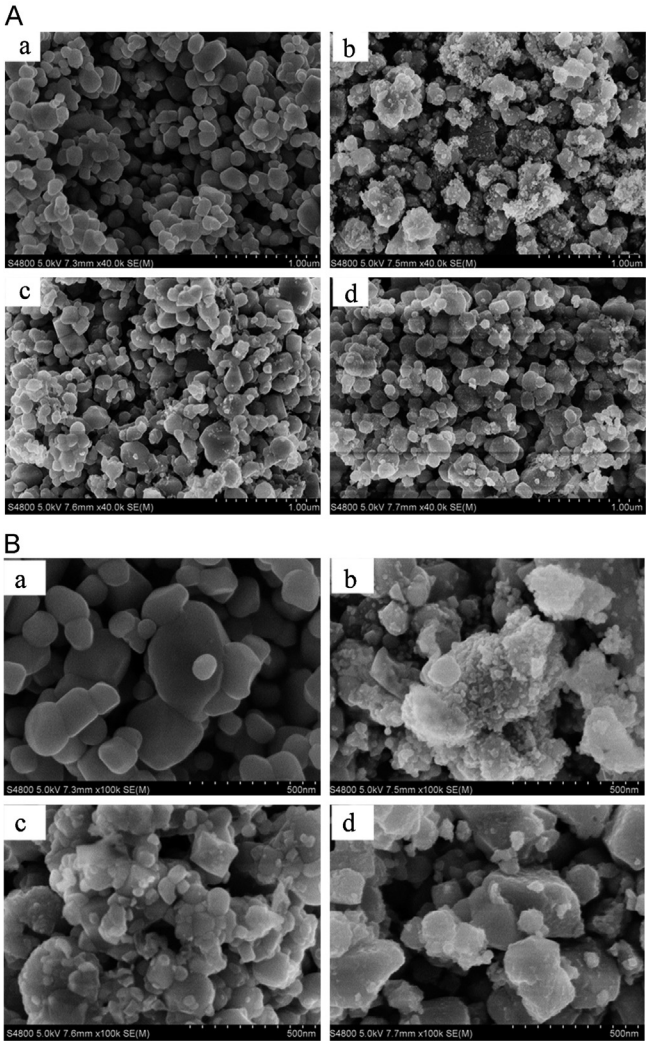

Fig. 3. SEM images of the catalysts: (a) TiO_2, (b) Fe(0.15)–Mn(0.3)/TiO_2, (c) Mn(0.3)/Fe(0.15)/TiO_2, and (d) Fe(0.15)/Mn(0.3)/TiO_2. (A) 40 000 multiplier and (B)100 000 multiplier.

Table 2. Percents of the surface atom were not equal despite three catalysts being prepared by using equal amount materials. Percentages of Fe, Mn and O on the surface of Fe(0.15)–Mn(0.3)/TiO_2 were higher than the others, which suggested one-step impregnation was useful for improving the dispersion of FeO_x and MnO_x on the surface of catalyst.

Fig. 4 showed the Mn 2p, Fe 2p, and O 1s photoelectron peaks of the catalysts measured by XPS. Distribution of the elements on the surface were obtained and listed in Table 3.

Through deconvolution of the spectra, three peaks of Mn $2p^{3/2}$ suggested the existence of three manganese states: Mn^{3+} at 641.5–641.7 eV [25,26], Mn^{4+} at 642.5 eV [25,26] and Mn-nitrate at 644.5 eV [27,28]. The Mn-nitrate peak was expected as the catalysts were calcined at a relatively low temperature of 450 °C [27,29]. Although the concentration of the surface atom Mn in Mn(0.3)/Fe(0.15)/TiO_2 was the lowest (10.54%), its percent of Mn^{3+} specie was very high (39.11%). Compared with the XRD results, it could be inferred that adding Fe before Mn would promote the generation of Mn_2O_3 but inhibit the dispersion of MnO_x on the surface of catalyst. Fe(0.15)–Mn(0.3)/TiO_2 which showed the maximum NO conversion possessed the highest Mn^{3+} percentage (39.18%), this phenomenon was also found in the other articles [14,25].

Table 2
Surface atom concentrations determined by XPS.

Samples	Percent of surface atomic by XPS (at%)			
	Ti	O	Fe	Mn
Fe(0.15)/Mn(0.3)/TiO_2	25.1	61.23	2.86	10.82
Mn(0.3)/Fe(0.15)/TiO_2	23.48	63.87	2.11	10.54
Fe(0.15)–Mn(0.3)/TiO_2	18.12	65	5.95	10.93

Fig. 4B showed the Fe 2p spectra of the samples. According to the results of deconvolution, the binding energies of Fe $2p^{3/2}$ were mainly centered at 711.4 eV which indicated that the majority of iron species in this sample was Fe^{3+} [30,31]. The peaks at 710 eV and 712.6 eV referred to Fe^{2+} cation [31,32] and Fe^{3+} bonded with hydroxyl group (Fe^{III}–OH) [19,32,33], respectively. The components observed at about 719 eV and 715.5 eV were the fingerprints of Fe^{3+} and Fe^{2+} species [33–35].

O 1s XPS spectra of all samples were asymmetric and fitted to the three groups. Lattice oxygen O^{2-} (denoted as O_β) and chemisorbed water (denoted as O_α') were located at 529.6–529.7 eV and 532.8 eV, respectively [5,36,37]. Peaks at 531.0–531.3 eV were assigned to surface adsorbed oxygen (denoted as O_α), such as O_2^{2-} and O^- belonged to defect-oxide or hydroxyl-like group [5,36,37]. O_α was often considered beneficial for the NO oxidation to NO_2 due to its higher mobility than O_β [5,24,25]. The concentration of O_α in Fe(0.15)–Mn(0.3)/TiO_2 sample was much higher compared with the other materials.

3.2. Effect of H_2O and SO_2 over Fe(0.15)–Mn(0.3)/TiO_2 catalyst

3.2.1. Sulfur tolerance and water resistance testing

It is difficult to remove SO_2 and H_2O completely from the flue gas. Thus, traces of SO_2 and H_2O may still exist and affect the denitrogen catalysis downstream [25,38]. The synergistic effects of SO_2 (200 ppm) and H_2O (4 vol%) on NO conversion over Fe(0.15)–Mn(0.3)/TiO_2 catalyst were investigated at 320 °C (Fig. 5).

When 4 vol% H_2O was added to the simulated flue gas, NO conversion decreased slowly and lost 7% activity in 160 min, but the activity recovered completely after the removing of H_2O. These results showed that the inhibiting effect of H_2O on the catalytic activity was reversible. Nevertheless, the NO_x conversion of Fe(0.15)–Mn(0.3)/TiO_2 decreased about 45% in 240 min with the adding of SO_2. When H_2O and SO_2 were added together, the NO conversion decreased to 16% which was the lowest spot. All those indicates that the NO oxidation activity of Fe(0.15)–Mn(0.3)/TiO_2 was intensively suppressed by the presence of SO_2. This result was consistent with the researches on other Mn and TiO_2 based catalysts [20,24,25,39–43]. Fig. 5 showed that the NO conversion recovered to 40% and 35% when SO_2 and H_2O were cut off. Therefore, after removing SO_2 and H_2O, the inhibiting effect on Fe(0.15)–Mn(0.3)/TiO_2 could be reduced. The deactivation of catalytic oxidation of NO with O_2 may mainly attribute to the deposition of metal sulfates. The adding SO_2 would be adsorbed and to form unstable sulfite ion on the surface of the catalyst as its adsorption capacity was stronger than that of NO on metal oxide [25]. The adsorbed oxygen then reacted with sulfite ion to form sulfate which could block the catalyst and inhibit the catalytic activity seriously [20,42].

3.2.2. FT-IR study

To gain insight for the adsorption characteristics of NO + O_2 and deactivation by H_2O and SO_2 during NO oxidation, the FT-IR spectra of co-adsorbed of NO (1000 ppm), O_2 (5%), H_2O (4 vol%) and SO_2 (500 ppm), over Fe(0.15)–Mn(0.3)/TiO_2 were investigated (Fig. 6). The sample was pretreated at 300 °C in N_2 for 2 h before exposing in the mixture gas for 2 h at 30 °C whose total flow rate was

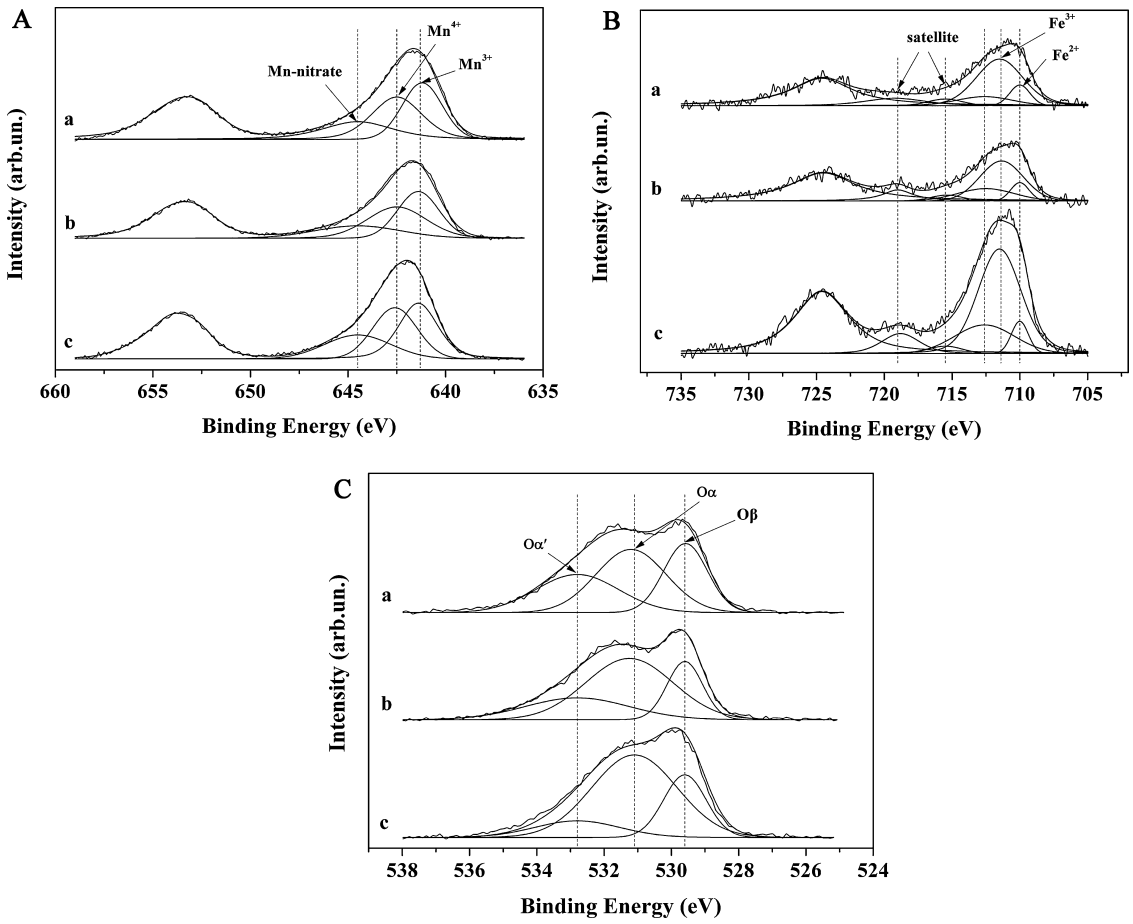

Fig. 4. XPS spectra of (A) Mn 2p; (B) Fe 2p; (C) O 1s for (a) Fe(0.15)/Mn(0.3)/TiO_2, (b) Mn(0.3)/Fe(0.15)/TiO_2, and (c) Fe(0.15)–Mn(0.3)/TiO_2.

300 ml/min, then purged it by N_2 at 80 °C for 1 h to remove the decomposition products.

There was obvious peaks at 1075 cm^{-1} was attributed to carbonate in Fig. 6a [44], it could be formed when the catalysts was exposed in the air. Other bands were different types of adsorbed NO_x species: bidentate nitrite (NO_2^-, 1394 cm^{-1}) [45] monodentate nitrate (NO_3^-, 1517 cm^{-1}), NO^- (1182 cm^{-1}) [46], and NO_2 species on the surface of catalyst (1642–1605 cm^{-1}) [46,47]. However, there was no trace of N_2O_3 and N_2O_4 located at 1885–1860 cm^{-1} and 1770–1740 cm^{-1} [48]. New peak at 1120 cm^{-1} corresponded to SO_4^{2-} was detected when SO_2 was added to the pretreating gas [49]. Meanwhile, it was not found when SO_2 was added with H_2O because it was covered by the peak of carbonate. A faint band was discernible at 1271 cm^{-1}, which has been assigned by others to molecularly adsorbed SO_2 [50].

As shown in Fig. 6c and d, different nitrate were formed: monodentate nitrate over the surface of catalyst (1540 cm^{-1}) [19,45], nitrate specie formed by the reaction of NO_2 and H_2O (1385 cm^{-1}) [18] and symmetric stretching of bidentate nitrite (1192 cm^{-1}) [45]. Peaks occurring at 1640 and 1394 cm^{-1} in Fig. 6a were both shifted approximately 8 cm^{-1} to 1632 and 1385 cm^{-1}. The results showed that when $NO + O_2$ was added with $H_2O + SO_2$, the formed nitrate on the surface of catalysts was more unstable and easier to decompose [51]. It could be inferred that H_2O and SO_2 in the flue gas would form SO_4^{2-} and decrease the binding force of NO_x with the surface of the catalyst.

Compared the FT-IR results with the sulfur and water tolerance tests, the inhibitory effect of H_2O and SO_2 on catalytic activity could be deduced. The existence of H_2O and SO_2 would block available active sites for the adsorption of NO, as their adsorptions on the catalyst were more competitive than NO [20,24,25]. The produced HNO_3 which was formed by the reaction of NO_2 and H_2O would also deposit on the catalysts' surface restrain the adsorption of NO [18]. When SO_2 existed in the flue gas, it would form metal sulfates with the metal on the surface of catalysts. The occupation of active site by sulfate species would consequently decrease the NO oxidation activity [20].

Table 3
Surface atomic ratio of catalysts determined by XPS.

XPS spectra	Surface atomic ratio, %			
	Element valence	Fe(0.15)/Mn(0.3)/TiO_2	Mn(0.3)/Fe(0.15)/TiO_2	Fe(0.15)–Mn(0.3)/TiO_2
Fe 2p	Fe^{2+}/Fe	12.93	12.18	7.72
	Fe^{3+}/Fe	71.74	62.70	68.20
Mn 2p	Mn^{3+}/Mn	36.86	39.11	39.18
	Mn^{4+}/Mn	38.31	39.21	35.71
O 1s	O_β/O	28.44	21.36	23.93
	O_α/O	41.78	55.25	63.39

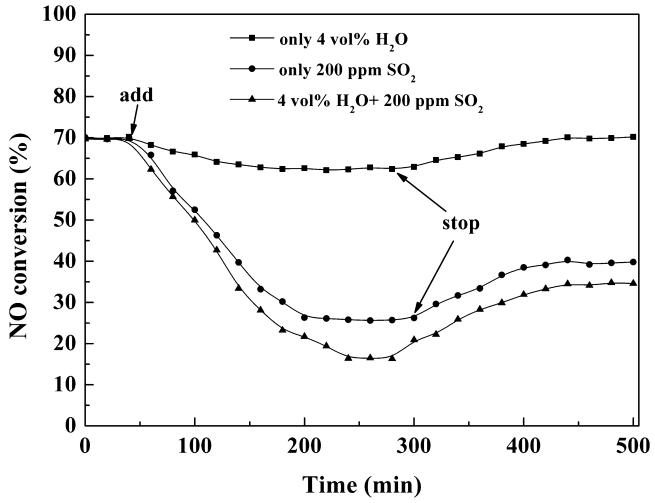

Fig. 5. Effect of H_2O and SO_2 on the NO conversion over Fe(0.15)–Mn(0.3)/TiO_2. Reaction conditions: 1.0 g sample, 500 ppm NO, 5% O_2, 4 vol% H_2O (when used), 200 ppm SO_2 (when used), N_2 balanced, at 320 °C; GHSV = 15 000 h^{-1}.

3.3. The mechanism study

3.3.1. Possible reaction mechanism over Fe(0.15)–Mn(0.3)/TiO_2

To further validate the gas–solid heterogeneous reaction between NO, O_2 and Fe(0.15)–Mn(0.3)/TiO_2, XPS measurement of the used sample (exposed to 2000 ppm NO and 10% O_2 for 4 h at the temperature of 320 °C) was also obtained. The percentages of core electrons for fresh and used sample were compared and listed in Fig. 7. The experimental results showed that the concentrations of Fe^{3+} and Mn^{3+} decreased, while the concentrations of the lower valence iron state (Fe^{2+}) and higher valence manganese state (Mn^{4+}) increased after 4 h reaction. Those results were corresponding with NO oxidation reactions over $Fe_3Mn_3O_8$ [18]. The electron transfer between Fe^{n+} and Mn^{n+} ions could be deduced in Eq. (1), and the following equations were presumed:

$$Fe^{3+} + Mn^{3+} \rightleftharpoons Fe^{2+} + Mn^{4+} \quad (1)$$

$$NO + Mn^{4+} \rightarrow NO_{ads}{}^{+} + Mn^{3+} \quad (2)$$

$$O_2 + 2Fe^{2+} \rightarrow 2Fe^{3+} + 2O_{ads}{}^{-} \quad (3)$$

$$NO_{ads}{}^{+} + O_{ads}{}^{-} \rightarrow NO_2 \quad (4)$$

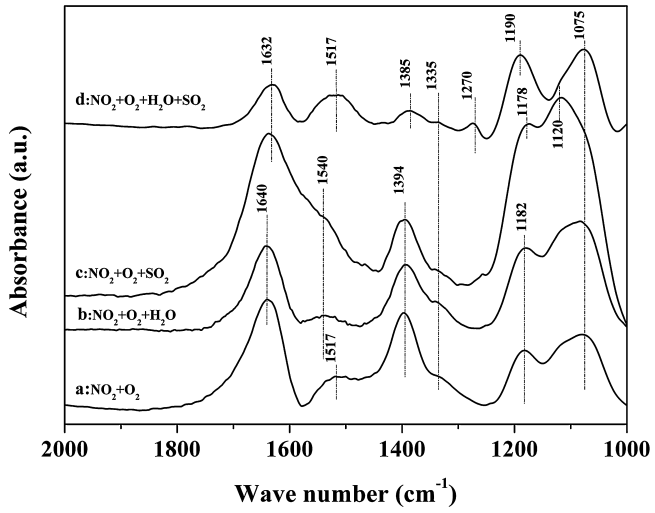

Fig. 6. FT-IR spectra taken upon Fe(0.15)–Mn(0.3)/TiO_2.

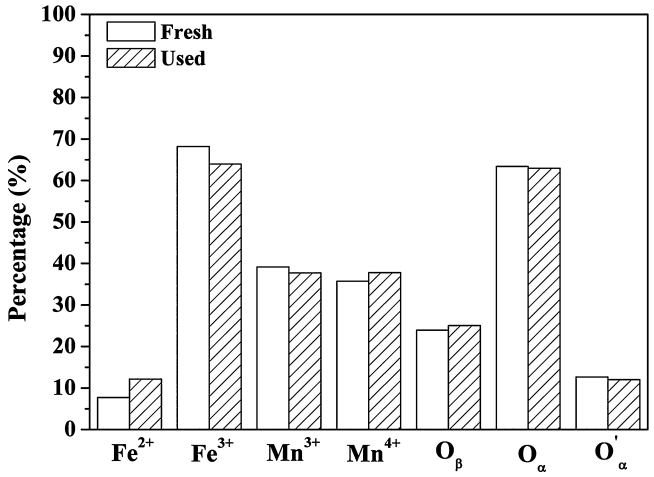

Fig. 7. Percentage of core electrons of used and fresh Fe(0.15)–Mn(0.3)/TiO_2.

The mechanism of oxidized NO with O_2 was extensively studied. It was believed that Eqs. (5) and (6) took place when the ration temperature was lower than 600 K [52].

$$2NO \rightleftharpoons (NO)_2 \quad (5)$$

$$(NO)_2 + O_2 \rightarrow 2NO_2 \quad (6)$$

Margarita Kantcheva indicated NO was firstly oxidized to NO_2, and then surface nitrates formed from NO_2 on the surface of TiO_2 [47]. The pathway of the formation of $NO_3{}^-$ was shown in Eqs. (7) and (8). Tang et al. and Li et al. proposed the NO was firstly oxidized to nitrates by lattice oxygen, then decomposed to NO_2 at high temperatures on Mn/TiO_2 and Ce-doped MnO_x/TiO_2 [15,18].

$$3NO + OH^- \rightarrow 2NO + NO^- + NOH \quad (7)$$

$$3NO_2 + 2OH^- \rightarrow 2NO_3{}^- + NO + H_2O \quad (8)$$

$$NO + O_2{}^- \rightarrow NO_3{}^- \quad (9)$$

$$NO + NO_3{}^- \rightarrow 2NO_2 + e^- \quad (10)$$

$$4NO_3{}^- \rightarrow 4NO_2 + O_2 + 2O^{2-} \quad (11)$$

Compared FT-IR results with the changes between increase and consumption of Fe^{n+} and Mn^{n+} ions between fresh and used catalysts, gasous NO might be oxidized by surface adsorbed oxygen and firstly formed NO_2 by the way in reactions (1)–(4). However, the formation of NO^- and bidentate nitrite on the surface suggested that gaseous NO could also formed bidentate nitrite as Eqs. (12)–(17). Besides, these reactions could happen at the same time.

$$NO + O_{ads}{}^- \rightarrow NO_2{}^- \quad (12)$$

$$NO_2{}^- + NO_2{}^- \rightarrow (NO_2)_2{}^{2-} \quad (13)$$

$$(NO_2)_2{}^{2-} \rightleftharpoons 2NO_2 \quad (14)$$

$$(NO_2)_2{}^{2-} + O_2 \rightarrow 2NO_3{}^- \quad (15)$$

$$2NO + O_{ads}{}^- \rightarrow NO_2 + NO^- \quad (16)$$

$$NO_2 + O_{ads}{}^- \rightarrow NO_3{}^- \quad (17)$$

As the reaction temperature was above 300 °C, the formed nitrates might decompose to gaseous NO_2 by processes 12–13 [53]. The mechanism of the NO oxidation reactions over Fe(0.15)–Mn(0.3)/TiO_2 were also proposed and depicted in Scheme 1.

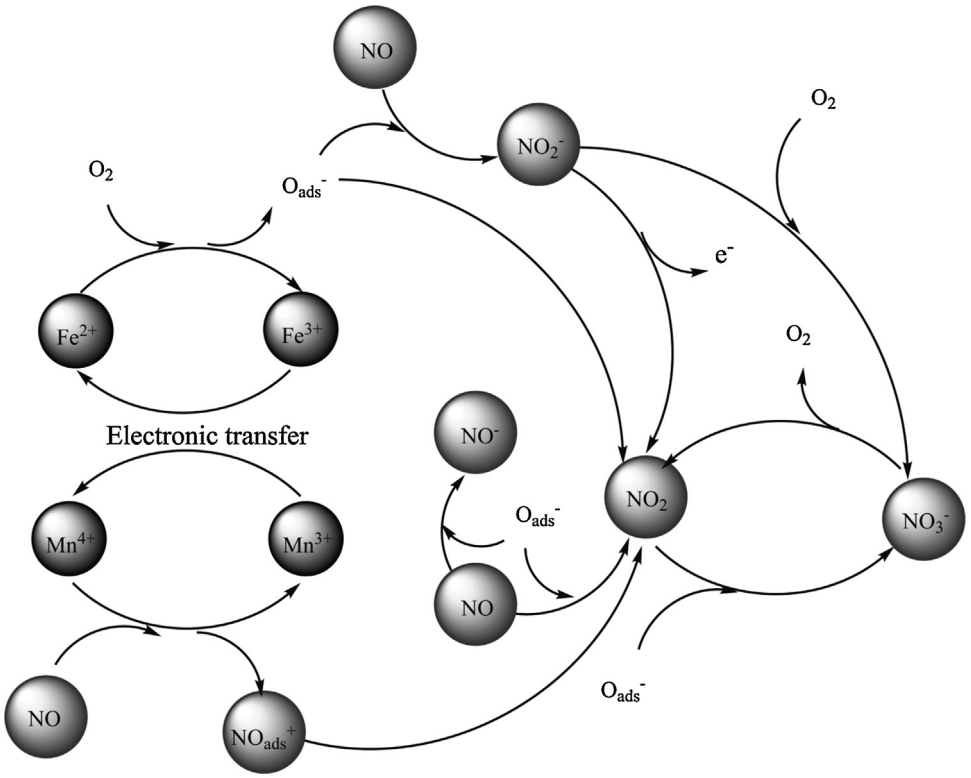

Scheme 1. Mechanism of the NO oxidation reactions over Fe(0.15)–Mn(0.3)/TiO_2.

4. Conclusions

This study not only aimed to explore the effect of loading sequences on the structure and activity of $FeMnO_x/TiO_2$, but also figured out the mechanism of NO oxidation over Fe(0.15)–Mn(0.3)/TiO_2. The conversion of NO to NO_2 yielded 70% at 320 °C with a space velocity of 15 000 h^{-1} with the catalyst prepared by one-step impregnation. Mn was important for catalytic activity on NO oxidation at low temperature. The results of BET, XRD and SEM characterizations indicated that the catalyst using one-step impregnation exhibited the largest surface area and best distribution of oxides on the support. The existence of Fe modified the structure of carriers, promoted the generation of Mn_2O_3 but inhibited its dispersion on the surface of catalysts. Analysis of XPS indicated that higher NO conversion might contribute to the increase of chemisorbed oxygen (O_α), Fe^{3+} and Mn^{3+}. The addition of SO_2 and H_2O in the feed gas could exert an adverse effect on the NO_x conversion. Comprehensive assessment of FT-IR and XPS results revealed the reaction mechanism that the gas NO might oxidized by adsorbed oxygen and firstly formed to NO_2 or bidentate nitrite on the surface of the catalyst.

Acknowledgments

The project is financially supported by the National Natural Science Foundation of China (51278177), the National High Technology Research and Development Program of China (863 Program, No. 2011AA060803) and the Scientific and Technological Major Special Project of Hunan Province in China (2010XK6003).

Appendix A. Supplementary data

Supplementary material related to this article can be found, in the online version, at http://dx.doi.org/10.1016/j.apsusc.2014.02.002.

References

[1] V.I. Pârvulescu, P. Grange, B. Delmon, Catalytic removal of NO, Catalysis Today 46 (1998) 233–316.
[2] C.F. You, X.C. Xu, Coal combustion and its pollution control in China, Energy 35 (2010) 4467–4472.
[3] S. Roy, M.S. Hegde, G. Madras, Catalysis for NO_x abatement, Applied Energy 86 (2009) 2283–2297.
[4] L.D. Li, Q. Shen, J. Cheng, Z.P. Hao, Catalytic oxidation of NO over TiO_2 supported platinum clusters. I: Preparation, characterization and catalytic properties, Applied Catalysis B: Environmental 93 (2010) 259–266.
[5] F.D. Liu, H. He, Y. Ding, C.B. Zhang, Effect of manganese substitution on the structure and activity of iron titanate catalyst for the selective catalytic reduction of NO with NH_3, Applied Catalysis B: Environmental 93 (2009) 194–204.
[6] I. Nova, C. Ciardelli, E. Tronconi, D. Chatterjee, B. Bandl-Konrad, NH_3-NO/NO_2 chemistry over V-based catalysts and its role in the mechanism of the Fast SCR reaction, Catalysis Today 114 (2006) 3–12.
[7] M. Sasaki, K. Suzuki, A. Sultana, M. Haneda, H. Hamada, Effect of acid–base properties on the catalytic activity of Pt/Al_2O_3 based catalysts for diesel NO oxidation, Topics in Catalysis 56 (2013) 205–209.
[8] S.K. Matam, E.V. Kondratenko, M.H. Aguirre, P. Hug, D. Rentsch, A. Winkler, A. Weidenkaff, D. Ferri, The impact of aging environment on the evolution of Al_2O_3 supported Pt nanoparticles and their NO oxidation activity, Applied Catalysis B: Environmental 129 (2013) 214–224.
[9] C.H. Shen, G.T. Rochelle, Nitrogen dioxide absorption and sulfite oxidation in aqueous sulfite, Environmental Science and Technology 32 (1998) 1994–2003.
[10] Z.B. Wu, Z.Y. Sheng, Y. Liu, H.Q. Wang, N. Tang, J. Wang, Characterization and activity of Pd-modified TiO_2 catalysts for photocatalytic oxidation of NO in gas phase, Journal of Hazardous Materials 164 (2009) 542–548.
[11] K. Li, X.L. Tang, H.H. Yi, P. Ning, Y. Xiang, J.G. Wang, C. Wang, X. Peng, Research on manganese oxide catalysts surface pretreated with non-thermal plasma for NO catalytic oxidation capacity enhancement, Applied Surface Science 264 (2013) 557–562.
[12] F. Kapteijn, L. Singoredjo, A. Andreini, J.A. Moulijn, Activity and selectivity of pure manganese oxides in the selective catalytic reduction of nitric oxide with ammonia, Applied Catalysis B: Environmental 3 (1994) 173–189.
[13] E. Park, S. Chin, J. Jeong, J. Jurng, Low-temperature NO oxidation over Mn/TiO_2 nanocomposite synthesized by chemical vapor condensation: effects of Mn precursor on the surface Mn species, Microporous and Mesoporous Materials 163 (2012) 96–101.
[14] Z.B. Wu, N.A. Tang, L. Xiao, Y. Liu, H.C. Wang, MnO_x/TiO_2 composite nanoxides synthesized by deposition–precipitation method as a superior catalyst for NO oxidation, Journal of Colloid and Interface Science 352 (2010) 143–148.
[15] N. Tang, Y. Liu, H.Q. Wang, Z.B. Wu, Mechanism study of NO catalytic oxidation over MnO_x/TiO_2 catalysts, Journal of Physical Chemistry C 115 (2011) 8214–8220.

[16] C.C. Zhou, Y.P. Zhang, X.L. Wang, H.T. Xu, K.Q. Sun, K. Shen, Influence of the addition of transition metals (Cr, Zr, Mo) on the properties of MnO_x–FeO_x catalysts for low-temperature selective catalytic reduction of NO_x by Ammonia, Journal of Colloid and Interface Science 392 (2013) 319–324.
[17] W.W. Zhao, C.T. Li, P. Lu, Q.B. Wen, Y.P. Zhao, X. Zhang, C.Z. Fan, S.S. Tao, Iron, lanthanum and manganese oxides loaded on γ-Al_2O_3 for selective catalytic reduction of NO with NH_3 at low temperature, Environmental Technology 34 (2013) 81–90.
[18] Z.H. Chen, F.R. Wang, H. Li, Q. Yang, L.F. Wang, X.H. Li, Low-temperature selective catalytic reduction of NO_x with NH_3 over Fe-Mn mixed-oxide catalysts containing $Fe_3Mn_3O_8$ phase, Industrial and Engineering Chemistry Research 51 (2012) 202–212.
[19] S.J. Yang, C.Z. Wang, J.H. Li, N.Q. Yan, L. Ma, H.Z. Chang, Low temperature selective catalytic reduction of NO with NH_3 over Mn–Fe spinel: performance, mechanism and kinetic study, Applied Catalysis B:Environmental 110 (2011) 71–80.
[20] J.F. Zhang, Y. Huang, X. Chen, Selective catalytic oxidation of NO over iron and manganese oxides supported on mesoporous silica, Journal of Natural Gas Chemistry 17 (2008) 273–277.
[21] Y.P. Zhang, X.L. Wang, K. Shen, H.T. Xu, K.Q. Sun, C.C. Zhou, WO_3 modification of MnO_x/TiO_2 catalysts for low temperature selective catalytic reduction of NO with ammonia, Chinese Journal of Catalysis 33 (2012) 1523–1531.
[22] Y.P. Zhang, X.Y. Zhao, H.T. Xu, K. Shen, C.C. Zhou, B. Jin, K.Q. Sun, Novel ultrasonic-modified MnO_x/TiO_2 for low-temperature selective catalytic reduction (SCR) of NO with ammonia, Journal of Colloid and Interface Science 361 (2011) 212–218.
[23] G. Pecchi, P. Reyes, T. López, R. Gómez, A. Moreno, J.L.G. Fierro, Effect of precursors on surface and catalytic properties of Fe/TiO_2 catalysts, Journal of Chemical Technology and Biotechnology 77 (2002) 944–949.
[24] J.X. Zhang, S.L. Zhang, W. Cai, Q. Zhong, The characterization of CrCe-doped on TiO_2-pillared clay nanocomposites for NO oxidation and the promotion effect of CeO_x, Applied Surface Science 268 (2013) 535–540.
[25] X.H. Li, S.L. Zhang, Y. Jia, X.X. Liu, Q. Zhong, Selective catalytic oxidation of NO with O_2 over Ce-doped MnO_x/TiO_2 catalysts, Journal of Natural Gas Chemistry 21 (2012) 17–24.
[26] B. Gillot, S. Buguet, E. Kester, C. Baubet, P. Tailhades, Cation valencies and distribution in the spinels $Co_xCu_yMn_zFe_uO_{4+\delta}$ ($\delta \geq 0$) thin films studied by X-ray photoelectron spectroscopy, Thin Solid Films 357 (1999) 223–231.
[27] D.A. Peña, B.S. Uphade, P.G. Smirniotis, TiO_2-supported metal oxide catalysts for low-temperature selective catalytic reduction of NO with NH_3. I: Evaluation and characterization of first row transition metals, Journal of Catalysis 221 (2004) 421–431.
[28] K.H. Park, S.M. Lee, S.S. Kim, D.W. Kwon, S.C. Hong, Reversibility of Mn valence state in MnO_x/TiO_2 catalysts for low-temperature selective catalytic reduction for NO with NH_3, Catalysis Letters 143 (2013) 246–253.
[29] J.H. Li, J.J. Chen, R. Ke, C.K. Luo, J.M. Hao, Effects of precursors on the surface Mn species and the activities for NO reduction over MnO_x/TiO_2 catalysts, Catalysis Communications 8 (2007) 1896–1900.
[30] V.M. Shinde, G. Madras, Low temperature CO oxidation and water gas shift reaction over Pt/Pd substituted in Fe/TiO_2 catalysts, International Journal of Hydrogen Energy 37 (2012) 18798–18814.
[31] J.R. Scheffe, A. Francés, D.M. King, X.H. Liang, B.A. Branch, A.S. Cavanagh, S.M. George, A.W. Weimer, Atomic layer deposition of iron(III) oxide on zirconia nanoparticles in a fluidized bed reactor using ferrocene and oxygen, Thin Solid Films 517 (2009) 1874–1879.
[32] C.L. Corkhill, P.L. Wincott, J.R. Lloyd, D.J. Vaughan, The oxidative dissolution of arsenopyrite (FeAsS) and enargite (Cu_3AsS_4) by Leptospirillum ferrooxidans, Geochimica et Cosmochimica Acta 72 (2008) 5616–5633.
[33] S.J. Yang, Y.F. Guo, N.Q. Yan, D.Q. Wu, H.P. He, J.K. Xie, Z. Qu, J.P. Jia, Remarkable effect of the incorporation of titanium on the catalytic activity and SO_2 poisoning resistance of magnetic Mn–Fe spinel for elemental mercury capture, Applied Catalysis B: Environmental 101 (2011) 698–708.
[34] M.V. Bukhtiyarova, A.S. Ivanova, L.M. Plyasova, G.S. Litvak, V.A. Rogov, V.V. Kaichev, E.M. Slavinskaya, P.A. Kuznetsov, I.A. Polukhina, Selective catalytic reduction of nitrogen oxide by ammonia on Mn(Fe)-substituted Sr(La) aluminates, Applied Catalysis A: General 357 (2009) 193–205.
[35] M. Descostes, F. Mercier, N. Thromat, C. Beaucaire, M. Gautier-Soyer, Use of XPS in the determination of chemical environment and oxidation state of iron and sulfur samples: constitution of a data basis in binding energies for Fe and S reference compounds and applications to the evidence of surface species of an oxidized pyrite in a carbonate medium, Applied Surface Science 165 (2000) 288–302.
[36] V.P. Santos, M.F.R. Pereira, J.J.M. Órfão, J.L. Figueiredo, The role of lattice oxygen on the activity of manganese oxides towards the oxidation of volatile organic compounds, Applied Catalysis B: Environmental 99 (2010) 353–363.
[37] W.P. Shan, F.D. Liu, H. He, X.Y. Shi, C.B. Zhang, A superior Ce–W–Ti mixed oxide catalyst for the selective catalytic reduction of NO_x with NH_3, Applied Catalysis B: Environmental 115–116 (2012) 100–106.
[38] Z.H. Chen, Q. Yang, H. Li, X.H. Li, L.F. Wang, S.C. Tsang, Cr-MnO_x mixed-oxide catalysts for selective catalytic reduction of NO_x with NH_3 at low temperature, Journal of Catalysis 276 (2010) 56–65.
[39] K. Li, X.L. Tang, H.H. Yi, P. Ning, D.J. Kang, C. Wang, Low-temperature catalytic oxidation of NO over Mn–Co–Ce–O_x catalyst, Chemical Engineering Journal 192 (2012) 99–104.
[40] B.X. Shen, Y. Yao, H.Q. Ma, T. Liu, Ceria modified MnO_x/TiO_2-pillared clays catalysts for selective catalytic reduction of NO with NH_3 at low temperature, Chinese Journal of Catalysis 32 (2011) 1803–1811.
[41] B.X. Shen, T. Liu, N. Zhao, X.Y. Yang, L.D. Deng, Iron-doped Mn–Ce/TiO_2 catalyst for low temperature selective catalytic reduction of NO with NH_3, Journal of Environmental Sciences 22 (2010) 1447–1454.
[42] R.B. Jin, Y. Liu, Z.B. Wu, H.Q. Wang, T.T. Gu, Relationship between SO_2 poisoning effects and reaction temperature for selective catalytic reduction of NO over Mn–Ce/TiO_2 catalyst, Catalysis Today 153 (2010) 84–89.
[43] B.Q. Jiang, Z.B. Wu, Y. Liu, S.C. Lee, W.K. Ho, DRIFT study of the SO_2 effect on low temperature SCR reaction over Fe–Mn/TiO_2, Journal of Physical Chemistry C 114 (2010) 4961–4965.
[44] S.J. Huang, A.B. Walters, M.A. Vannice, Adsorption and decomposition of NO on lanthanum oxide, Journal of Catalysis 192 (2000) 29–47.
[45] J.C.S. Wu, Y.T. Cheng, In situ FTIR study of photocatalytic NO reaction on photocatalysts under UV irradiation, Journal of Catalysis 237 (2006) 393–404.
[46] G.S. Qi, R.T. Yang, R. Chang, MnO_x-CeO_2 mixed oxides prepared by co-precipitation for selective catalytic reduction of NO with NH_3 at low temperatures, Applied Catalysis B: Environmental 51 (2004) 93–106.
[47] M. Kantcheva, Identification, stability, and reactivity of NO_x species adsorbed on titania-supported manganese catalysts, Journal of Catalysis 204 (2001) 479–494.
[48] M. Iwasaki, H. Shinjoh, NO evolution reaction with NO_2 adsorption over Fe/ZSM-5: in situ FT-IR observation and relationships with Fe sites, Journal of Catalysis 273 (2010) 29–38.
[49] I. Labádi, L. Horváth, G. Kenessey, G. Liptay, Preparation, thermoanalytical and IR study of mixed-ligand complexes formed in water-1,2-ethanediol-cobalt(II)sulfate systems, Journal of Thermal Analysis and Calorimetry 83 (2006) 247–251.
[50] C. Quijada, A. Rodes, J.L. Vázquez, J.M. Pérez, A. Aldaz, Electrochemical behaviour of aqueous SO_2 at Pt electrodes in acidic medium. A voltammetric and in situ Fourier transform IR study. Part I: Oxidation of SO_2 on Pt electrodes with sulphur-oxyge adsorbed species, Journal of Electroanalytical Chemistry 394 (1995) 217–227.
[51] B.X. Shen, X.P. Zhang, H.Q. Ma, Y. Yao, T. Liu, A comparative study of Mn/CeO_2, Mn/ZrO_2 and Mn/Ce–ZrO_2 for low temperature selective catalytic reduction of NO with NH_3 in the presence of SO_2 and H_2O, Journal of Environmental Sciences – China 25 (2013) 791–800.
[52] J. Olbregts, Termolecular reaction of nitrogen monoxide and oxygen a still unsolved problem, International Journal of Chemical Kinetics 17 (1985) 835–848.
[53] R. Brosius, D. Habermacher, J.A. Martens, L. Vradman, M. Herskowitz, L. Capek, Z. Sobalik, J. Dedecek, B. Wichterlova, V. Tokarova, O. Gonsiorova, NO oxidation kinetics on iron zeolites: influence of framework type and iron speciation, Topics in Catalysis 30 (2004) 333–339.